frontiers | Frontiers in Energy Research

TYPE Original Research
PUBLISHED 15 September 2022
DOI 10.3389/fenrg.2022.971357

OPEN ACCESS

EDITED BY
Chi-Man Vong,
University of Macau, China

REVIEWED BY
Jichao Hong,
University of Science and Technology Beijing, China
Shaobo Xie,
Chang'an University, China

*CORRESPONDENCE
Mokhtar Shouran,
shouranma@cardiff.ac.uk

SPECIALTY SECTION
This article was submitted to ExSmart Grids,
a section of the journal
Frontiers in Energy Research

RECEIVED 17 June 2022
ACCEPTED 19 August 2022
PUBLISHED 15 September 2022

CITATION
Oubelaid A, Taib N, Rekioua T, Bajaj M, Yadav A, Shouran M and Kamel S (2022), Secure power management strategy for direct torque controlled fuel cell/supercapacitor electric vehicles. *Front. Energy Res.* 10:971357. doi: 10.3389/fenrg.2022.971357

Secure power management strategy for direct torque controlled fuel cell/supercapacitor electric vehicles

Adel Oubelaid[1], Nabil Taib[1], Toufik Rekioua[1], Mohit Bajaj[2], Arvind Yadav[3], Mokhtar Shouran[4]* and Salah Kamel[5]

[1]Laboratoire de Technologie Industrielle et de l'Information, Faculté de Technologie, Université de Bejaia, Bejaia, Algeria, [2]Department of Electrical Engineering, Graphic Era (Deemed to Be University), Dehradun, India, [3]Department of Electrical Engineering, GLA University, Mathura, India, [4]Wolfson Centre for Magnetics, School of Engineering, Cardiff University, Cardiff, United Kingdom, [5]Department of Electrical Engineering, Faculty of Engineering, Aswan University, Aswan, Egypt

High reliability is recommended in hybrid electric vehicle applications. In this study, a secure power management strategy has been developed for a fuel cell—supercapacitor hybrid electric vehicle. In addition to its ability to detect the occurrence of failures in vehicle power sources, the proposed power management strategy isolates the faulty source and reconfigures the control scheme to always guarantee bus voltage stability and vehicle traction even in faulty situations. The developed power management strategy enhances vehicle comfort and prevents exhausting one source over another by allowing the fuel cell and the supercapacitor to operate at different power levels. The multiloop control scheme associated with the power sources is highly reliable since both sources can run the vehicle alone and regulate the bus voltage. Vehicle speed and torque controllers are simultaneously tuned using a particle swarm optimization algorithm. Torque and speed ripples are automatically minimized *via* the use of a new proposed cost function. This approach made the controller design easier and gave the designer the possibility to tradeoff between the variables to be minimized.

KEYWORDS

hybrid electric vehicle, secure power management, particle swarm optimization, fuel cell, supercapacitor

1 Introduction

In the last decade, several studies were carried out to investigate alternative nonpolluting energy sources to solve the persisting problem of carbon emission. Vehicle electrification was among the proposed solutions for the elimination or at least the reduction of gas emission. This solution has attracted many researchers and different research axes have been born out of the increasing interest given to this idea, such as vehicle safety and security (Sabaliauskaite et al., 2019), energy management (Zhang et al., 2017a; Yadav and Maurya, 2021a; Yadav and Maurya, 2021b; Yadav and

Maurya, 2022), power sources protections (Oubelaid et al., 2022a), power train architecture (Wu et al., 2015), intelligent transportation (Oubelaid et al., 2022b; Oubelaid et al., 2022c), and vehicle control (Max and Lantos, 2014; Vajsz et al., 2017; Oubelaid et al., 2022d).

Hybrid electric vehicles can be thought of as mobile embedded systems that are subjected to unpredictable driving conditions. Knowing that environmental driving conditions are harsh and random, hybrid electric vehicles are permanently subjected to failure risk, which may be due to a fault in one of their components. Several research studies discussing the enhancement of hybrid electric vehicle security are available in the literature. To ensure continuous vehicle operation, researchers use different fault tolerant strategies which are applied to different hybrid electric vehicle components. Yu et al. (2017), Kersten et al. (2019), and Moosavi et al. (2019) have discussed possible open circuit faults occurring in inverters used in electrified vehicles. Faults taking place in traction machines and ensuring electric vehicle traction are also extensively studied in the literature. Mellor et al. (2003), Tashakori and Ektesabi (2013), Kaplan et al. (2021), Liu et al. (2021), and Wu et al. (2022) have proposed fault tolerant control strategies to handle possible faults in vehicle traction machine and ensure continuous and secure operation. Faults which may occur in the different sensors on vehicle boards are also extensively studied in the literature (Kommuri et al., 2016; Peñate et al., 2018; Yu et al., 2021; Zhang et al., 2021). To summarize, although inverters, traction machines, and sensors are more robust compared to fuel cells and supercapacitors, few research works have dealt with possible faults at the vehicle power sources level, except for some works which have mainly discussed power sources degradation (Shchurov et al., 2021; Song et al., 2021; Yi et al., 2022).

As mentioned earlier, vehicle power sources such as fuel cells are too sensitive. In addition, hybrid electric vehicles are always subjected to fast and abrupt load variations which could result in significant damage at both the source and motor sides. For the aforementioned reason, scientists have increased their efforts in developing novel control techniques which protect sensitive power sources such as fuel cells from possible damage due to sudden load variations. Ou et al. (2017) proposed a novel control technique that protects FC from overheating and air starvation that may be caused by rapid load variation. Koprivsek (2018) developed an over-current protection strategy to protect the battery electric vehicles from high currents resulting from rapid load variations. Liu et al. (2017) and Zhang et al. (2020) presented filter based control technique to protect both fuel cells and batteries from transient current ripples arising during abrupt power reference variation caused by abrupt load variations using rate limiters and a first-order transfer function to restrict fuel cell and battery output power and to produce a time delay necessary for the electrochemical reactions that occur within the FC. To conclude, vehicle power sources are so sensitive, and their failure possibility has to be taken into account when elaborating on control techniques or power management strategies.

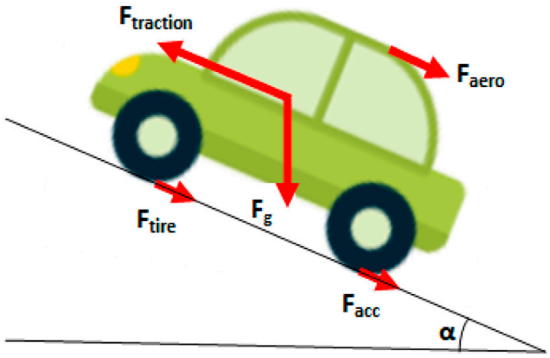

FIGURE 1
HEV in inclined surface.

Recently developed power management strategies for hybrid electric vehicles take into account the sensitivity and slowness of some vehicle power sources, such as fuel cells, but do not consider their possible failure. Ou et al. (2019) proposed a novel energy management technique based on fuzzy logic and state machine control techniques to enhance FC lifespan. He et al. (2020), Tao et al. (2020), and Trinh and Ahn (2021) developed energy management strategies that take into account only FC slow dynamics but do not consider its possible failure, and this reduces driving security. In many research works (Thounthong et al., 2009; Hwang et al., 2012; Zhang et al., 2017b; Wieczorek and Lewandowski, 2017; Meyer et al., 2018; Xie et al., 2018; Zhang et al., 2018; Raghavaiah and Srinivasarao, 2019; Kakouche et al., 2022), one power source always performs DC bus regulation, and the second source intervenes either during regenerative braking or to help the primary source during accelerations and high power demands. In case of failure of the sources fixing the DC bus voltage, the vehicle will lose its main powering source, and this may lead to serious vehicle damages and even total vehicle failure.

In this study, a novel power management strategy that takes into account possible failures in vehicle power sources is presented in this work. Unlike the previously mentioned power sharing techniques, the proposed management strategy offers the following advantages:

- Precise power flow control since, at any driving instant, the fuel cell can deliver any desired fraction of the total power required for traction
- Power sources are operated at known and defined operating points, and this reduces the stress applied on them during high power demands and, hence, increases their lifespan.

TABLE 1 HEV parameters.

Parameter	Value
Weight	1,200 Kg
Wheel radius	0.32 m
Maximum torque	126 N m
Frontal area	2.6 m^2
Air density	1.2 kg/m^3
Aerodynamic coefficient	0.3

- Secure vehicle operation: a fault detection algorithm will detect possible failures in vehicle power sources and correct them *via* control loop reconfiguration.

Hybrid electric vehicle traction is ensured using direct torque control–based space vector modulation. All vehicle regulators are concurrently tuned using a particle swarm optimization algorithm. This aforementioned intelligent technique permits simultaneous tuning through the use of newly proposed cost functions that allows the designer to tradeoff and prioritize between the design variables to be minimized.

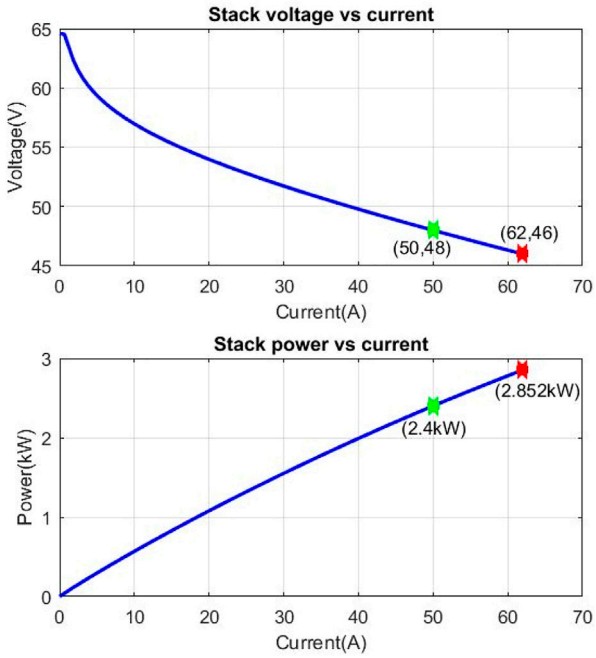

FIGURE 2
Fuel cell characteristic curves.

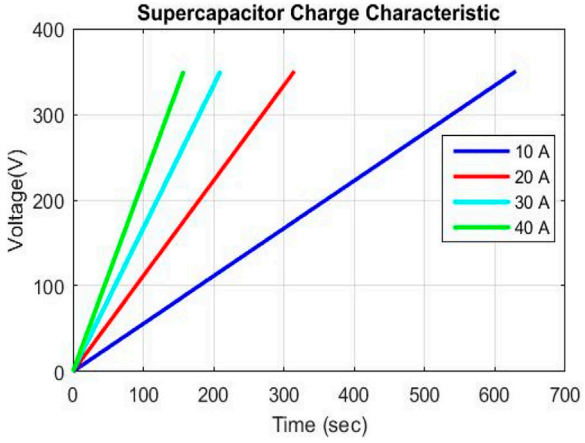

FIGURE 3
Supercapacitor characteristic curve.

2 Vehicle dynamics

The motion of the vehicle shown in Figure 1 is governed by the following equation:

$$\vec{F}_{traction} - \vec{F}_r = m\vec{a}, \tag{1}$$

where $\vec{F}_{traction}$is the net external force acting on the vehicle body, $\vec{F}_r$ is the net resistive force, m is the vehicle mass, and $\vec{a}$ is the vehicle acceleration vector.

The net resistive force is defined as given below:

$$\vec{F}_r = \vec{F}_{aero+}\vec{F}_g + \vec{F}_{tire} + \vec{F}_{acc}, \tag{2}$$

where F_{aero} is the aerodynamic force, F_g is the force due to gravity, F_{tire} is the friction force which exists between the vehicle's tire and ground surface, and F_{acc} is the acceleration force required by the vehicle to reach maximum speed from rest. Details about the mathematical modeling of each force are provided in the study by Shchurov et al. (2021). Vehicle parameters which are used in this study are shown in Table1.

3 Power sources modeling

3.1 FC modeling

The output voltage of one fuel cell (FC) is given by Eq. 3, which is approximately equal to 0.7 V. From this equation, one can notice the existence of several voltage drops, such as activation, ohm, and conduction voltage drops. More information about FC dynamics is given in the study by Song et al. (2021). From Eq. 4, the voltage of one FC stack is formed by serial grouping of N_s = 68, which makes the stack nominal voltage approximately 48 V.

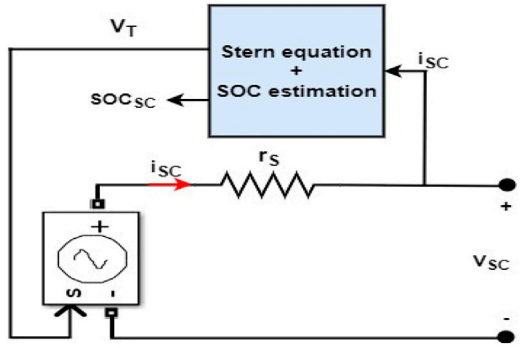

FIGURE 4
Electrical supercapacitor equivalent model.

$$V_{FC,cell} = E_{nernst} - V_{act} - V_{ohm} - V_{cond}, \quad (3)$$

$$V_{FC} = N_S V_{FC,cell}. \quad (4)$$

The voltage-current characteristic and power-current characteristics of one fuel cell stack are highlighted in Figure 2. The green points on the curves represent the nominal current, voltage, and power of the used FC.

3.2 SC modeling

The supercapacitor (SC) is used along with the fuel cell to make up for the FC's slow dynamics and also to increase vehicle performance. In addition to their fast dynamics, SCs are known for their robustness and their high number of charge and discharge cycles. Figure 3 shows the SC characteristic curve where one can notice that it gets charged very fast and sustains very high charge currents.

The electrical SC equivalent circuit is shown in Figure 4. It is modeled as a controlled voltage source in series with an equivalent series resistance, as shown next.

SC cell voltage V_{SC} is calculated by Eq. 5 using the Stern equation. Details about this last-mentioned equation are provided in the study by Yi et al. (2022). The SC state of charge (SOC_{SC}) is calculated by Eq. 6 using the initial and the total SC charges, Q_{init} and Q_T, respectively.

$$V_{SC} = V_T - r_{sc} i_{sc}, \quad (5)$$

$$SOC_{SC} = 100 * \frac{Q_{init} - \int_0^t i(\tau) d\tau}{Q_T}. \quad (6)$$

The total SC stack voltage is given by Eq. 7:

$$V_{SC,tot} = N_{SC} V_{SC}, \quad (7)$$

where $V_{sc,\ tot}$ is the total SC voltage, V_{sc} is the SC cell voltage, and N_{sc} is number of series supercapacitors.

TABLE 2 HEV and environment parameters.

Parameter	Value
P	35 kW
T_n	111 N.m
r_s	0.05 Ω
L	6.35 mH
ϕ	0.192 Wb
J	0.011 kg m^2
B	0.002 N.m.s
P	4

4 HEV traction and control

4.1 HEV traction

Permanent magnet synchronous machine (PMSM) is used to ensure HEV traction. It is chosen among other types of machines because of its robustness and its high torque to mass ratio, which means that it can deliver high torque and occupy small place in the space at the same time.

Stator flux and currents of PMSM motor in the dq rotating frame are, respectively, given by Eq. 8 and Eq. 9:

$$\begin{cases} \lambda_d = L i_d + \phi \\ \lambda_q = L i_q \end{cases}, \quad (8)$$

$$\begin{cases} \frac{di_d}{dt} = -\frac{r_s}{L} i_d + \frac{V_d}{L} + p w_r i_q \\ \frac{di_q}{dt} = -\frac{r_s}{L} i_q + \frac{V_q}{L} - p w_r i_d - \frac{\phi w_r}{L} \end{cases}, \quad (9)$$

where r_S and L are the stator resistance and inductance, respectively.ϕ is the flux of the permanent magnet. More information about PMSM is provided in the study by Jnayah and Khedher (2019). The parameters of the PMSM motor used in this work are shown in Table 2.

4.2 HEV control

The HEV discussed in this study is shown in Figure 5. It can be seen that the traction machine is controlled using direct torque control–based space vector modulation This control technique was chosen on purpose because of the fast torque response it provides.

At each sampling time Ts, the flux on the αβ frame and flux magnitude are estimated using Eq. 10 and Eq. 11. It is worth noticing that the PMSM stator resistance was neglected during flux estimation. Eq. 12 and Eq. 13 are used to estimate PMSM torque and rotor angle, respectively.

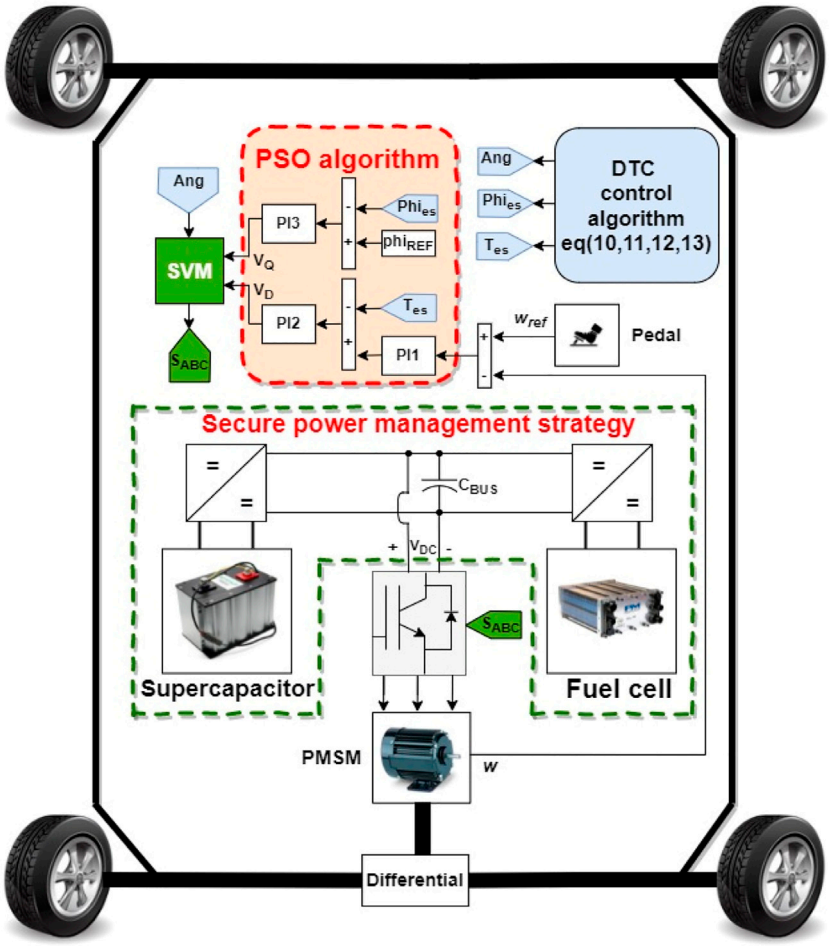

FIGURE 5
Top view of SC-FC HEV.

$$\begin{cases} \phi_\alpha[k+1] = \phi_\alpha[k] + T_s{}^*V_\alpha[k] \\ \phi_\beta[k+1] = \phi_\beta[k] + T_s V_\beta[k] \end{cases}, \tag{10}$$

$$\phi_{es}[k+1] = \sqrt{\phi_\alpha^2[k+1] + \phi_\beta^2[k+1]}, \tag{11}$$

$$T_{es} = 1.5p\left(\varnothing_\alpha i_\beta - \varnothing_\beta i_\alpha\right), \tag{12}$$

$$\theta_s[k+1] = tan^{-1}\left(\frac{\phi_\beta[k+1]}{\phi_\alpha[k+1]}\right). \tag{13}$$

Figure 6 presents the steps followed for the integration of particle swarm optimization (PSO) along with the DTC control technique. PSO is used offline to provide a self-tuning for HEV regulators: PI1, PI2, and PI3.

The steps for the integration of this optimization technique into the HEV control system are as follows:

- Initialize the swarm in a six-dimension search space.
- For each population particle, run the HEV system for a complete speed profile and evaluate the particle's performance using the following cost function:

$$J = \left(\overline{AASE} + \overline{AATE}\right). \tag{14}$$

$\overline{\text{AASE}}$ is the average absolute speed error and $\overline{\text{AATE}}$ is the average absolute torque error, which are, respectively, calculated by Eqs 15 and 16, where Ω_i and T_i are the reference speed and torque at each sampling time T_s. $\widehat{\Omega}_i$ and $\widehat{T}_i$ represent the measured HEV speed and torque, respectively. N is the length of the torque and speed vectors, and it is given by Eq. 7. T_d is the duration of the speed profile

$$\overline{AASE} = \frac{1}{N}\sum_{k=1}^{N}\left|\Omega_i - \widehat{\Omega}_i\right|, \tag{15}$$

$$\overline{AATE} = \frac{1}{N}\sum_{k=1}^{N}\left|T_i - \widehat{T}_i\right|, \tag{16}$$

$$N = T_s T_d. \tag{17}$$

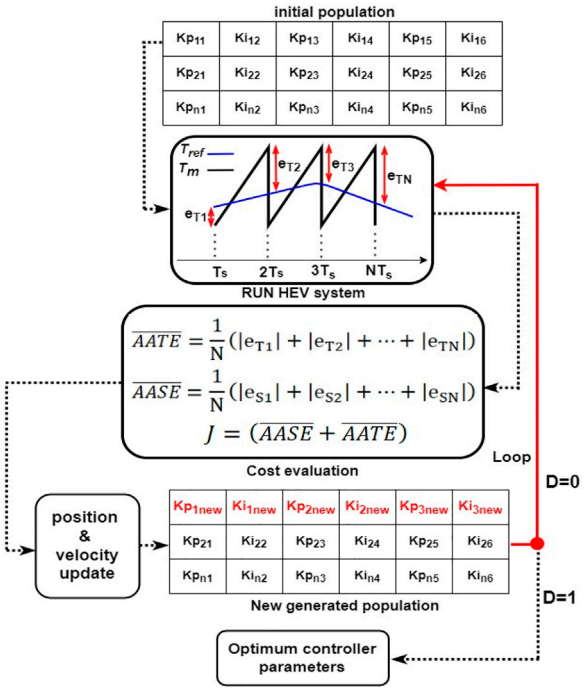

FIGURE 6
Integration of PSO to the HEV control system.

TABLE 3 Particle swarm optimization parameters.

Parameter	Population size	Number iteration	C1	C2
Value	50	50	0.5	0.5

- Apply penalty function to exclude unstable PI combinations that result in infinite cost values. Infinite or large cost values mean that the actual PMSM speed or torque values are too far from their references.
- Update the particle's speed and position using Eq. 18 and Eq. 19, respectively

$$v_i^{t+1} = w_t v_i^t + c_1 r_1 \left[P_{best}^t - x_i^t\right] + c_2 r_2 \left[G_{best}^t - x_i^t\right], \quad (18)$$

$$x_i^{t+1} = x_i^t + v_i^{t+1}. \quad (19)$$

- Evaluate the cost of the particle at its new location. If it is smaller than the previous cost value, then update it
- Keep iterating until the decision signal D (Figure 6) is 1. This last-mentioned signal is equal to 1 when the maximum number of iterations is elapsed or the minimum cost is reached.
- Extract the best position resulting in the smallest cost value.

The used PSO parameters in this study are highlighted in Table 3.

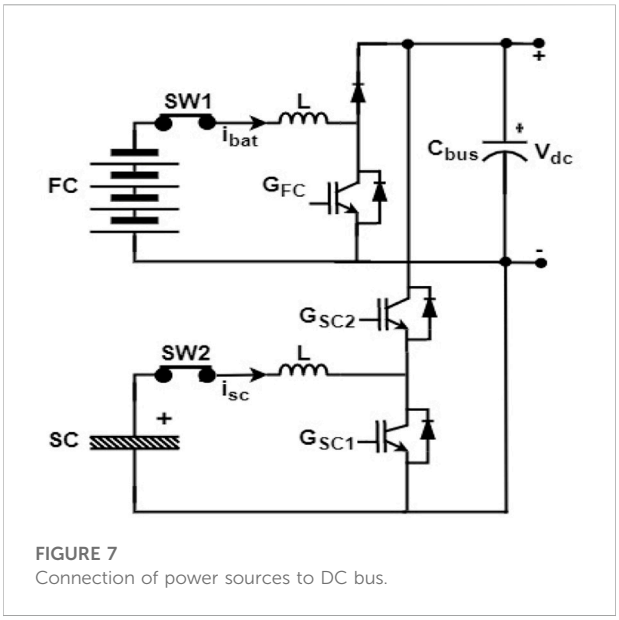

FIGURE 7
Connection of power sources to DC bus.

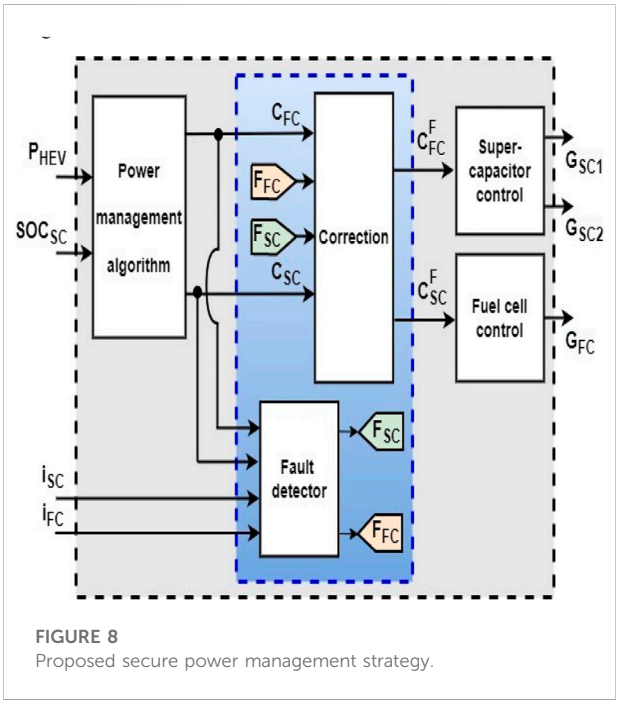

FIGURE 8
Proposed secure power management strategy.

5 Secure power management strategy

The connection of the SC and FC to the inverter DC bus is made, respectively, through bidirectional and unidirectional DC/DC converters, as shown in Figure 7.

As mentioned earlier, SC and FC have complementary characteristics. This is why their use has to be managed to ensure driving comfort and good vehicle performance.

Figure 8 highlights a top-level view of the proposed fault-tolerant power management strategy developed in this study. This bloc takes as inputs the power required by the HEV P_{HEV}, supercapacitor current i_{SC} and its SOC and FC current. It outputs three gate signals that control the operation of the power sources through the control of DC/DC converters gate signals.

The blue highlighted area in Figure 8 is used for the detection of faults that may occur in HEV power sources. If the SC or FC is in a failure state, this bloc will detect the fault and isolate it. After that, it will reconfigure the control loops associated with the power sources to ensure HEV traction and DC bus regulation. Details about this bloc are discussed in the coming sections. The signals N_{FC} and N_{SC} are called initial control signals, and A and B are considered final control signals.

5.1 Power management algorithm

In this work, the required HEV power is divided into three sets: low-power P_L, average-power P_A and high-power P_H. The supercapacitor SOC is divided into four levels, as given by Eq. 20:

$$SOC_{SC} = \begin{cases} SOC_H \, if \;\; 80 \le SOC_{SC} \le 90 \\ SOC_N \, if \;\; 65 \le SOC_{SC} < 80 \\ SOC_A \, if \;\; 50 \le SOC_{SC} < 65 \\ SOC_L \, if \;\; 0 \le SOC_{SC} < 50 \end{cases}. \tag{20}$$

The power management algorithm sub bloc highlighted in Figure 8 takes as input the required HEV power and the supercapacitor SOC and outputs two initial control signals N_{FC} and N_{SC} which are integers ranging from 1 to 4. These two last mentioned signals will be used to control the flow of power in FC and SC during normal HEV operation (absence of failures in HEV power sources). The table below presents different rules that are used by the power the management algorithm unit shown in Figure 8.

From the Table 4 the following subsections, one can notice that the proposed energy management not only switches ON and OFF the power sources but also controls the percentage of power delivered by each source, as shown in the following sub-sections:

5.2 Fuel cell control

The flow of power in the FC is controlled using the control scheme shown in Figure 9. Four loops are connected to a multiport switch, whose output depends on the final control signal C_{FC}^F, which is an integer variable ranging from 1 to 4. The control signal G_{FC} will trigger ON and OFF the gate of the DC/DC converter associated with the FC to control the flow of power on it.

If C_{FC}^F equals 2, $i_{fc,ref} = i_{fc,ref2}$, and the FC will provide 70% of the required power.

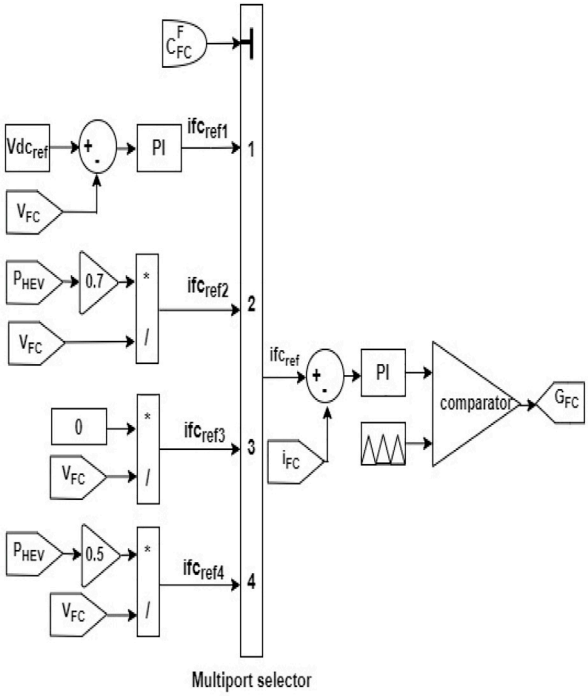

FIGURE 9
FC control scheme. If C_{FC}^F equals 1, $i_{fc,ref} = i_{fc,ref1}$, and the FC will ensure DC bus regulation.

If C_{FC}^F equals 3, $i_{fc,ref} = i_{fc,ref3}$, and the FC will be turned OFF or isolated (disconnected).

If C_{FC}^F equals 4, $i_{fc,ref} = i_{fc,ref4}$, and the FC will deliver 50% of the required power.

5.3 Supercapacitor control

The SC control scheme is shown in Figure 10. Multiple SC reference currents are connected to a multiport switch, whose output depends on the final control signal C_{SC}^F, which is an integer variable ranging from 1 to 4.

If C_{SC}^F equals 1, $i_{sc,ref} = i_{sc,ref1}$, and the SC will ensure DC bus regulation.

If C_{SC}^F equals 2, $i_{sc,ref} = i_{sc,ref2}$, and the SC will be charge under different modes.

If C_{SC}^F equals 3, $i_{sc,ref} = i_{sc,ref3}$, and the SC will be turned OFF or isolated (disconnected).

If C_{SC}^F equals 4, $i_{sc,ref} = i_{sc,ref4}$, and the SC will deliver its maximum power.

5.3.1 Supercapacitor charging

The dashed red lines of Figure 10 show the SC charging bloc, which takes as input the SC voltage and its SOC. Eq. 21 presents the two SC charging modes depending on the SOC. These two

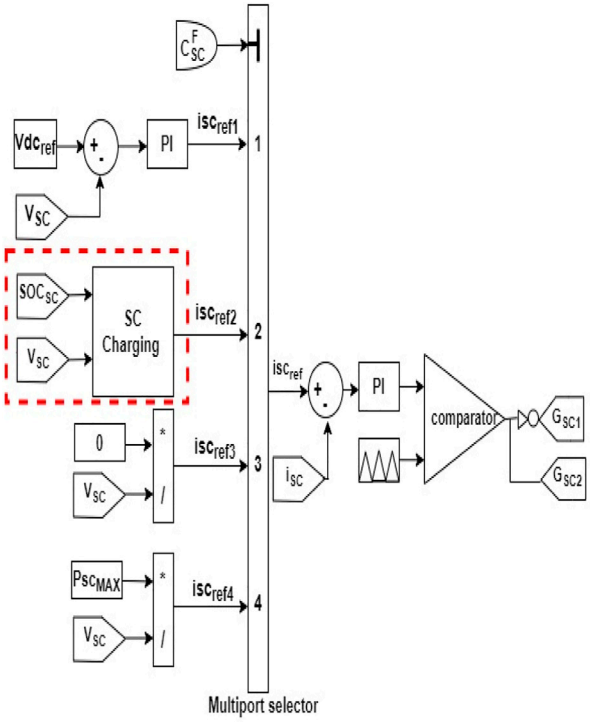

FIGURE 10
SC control scheme.

formulas limit the charging currents and prevent the SC from damage caused by current abrupt peaks.

$$i_{SC,ref} = \begin{cases} \dfrac{0.45P_{SC,max}}{V_{SC}} \; if \; SOC_L \le SOC_{SC} < SOC_H \\ \dfrac{0.7P_{SC,max}}{V_{SC}} \quad if \; SOC_{SC} < SOC_L \end{cases} . \tag{21}$$

5.3 Fault detection and correction

While FC or SC is operating alone (mode 1, 2, 5, and 13), the initial control signal of the other nonoperating source (C_{FC} or C_{SC}) will be set to 3 for it to be off, as can be deduced from Table 4. So, a given source is in a failure state if its current is null and its initial control signal generated by the power management algorithm is different from 3.

The used function for the detection of any possible fault in the FC is given by the following equation:

$$F_{FC} = \begin{cases} 1; \; if \; C_{FC} \neq 3 \; and \; i_{FC} = 0) \\ 0 \qquad otherwise \end{cases} . \tag{22}$$

In order to detect faults on SC, the following equation is used:

$$F_{SC} = \begin{cases} 1; \; if \; (C_{SC} \neq 3 \; \& \; and \; i_{SC} = 0) \\ 0 \qquad otherwise \end{cases} . \tag{23}$$

Once a fault is detected, the faulty source will be isolated, and the HEV must keep running by relying only on one source. When a fault occurs, the fault correction bloc, shown in Figure 8, uses the following truth table to reconfigure the control scheme and to isolate the faulty source. The correction bloc outputs two control signals C^F_{FC} and C^F_{SC}, which will control the state of SW1 and SW2 and the power flow in SC and FC.

From the Table 4 the following subsections, it can be seen that, in the absence of faults ($F_{SC} = F_{FC} = 0$), the isolation bloc outputs directly the initial control signals generated by the management algorithm bloc and behaves as IN-OUT bloc. When a fault occurs, the final control signal of the non-faulty source (C^F_{FC} orC^F_{SC}) will be set to 1 to guarantee DC bus voltage stability, and the faulty source control signal (C^F_{FC} orC^F_{SC}) will be set to 3 to isolate it, as shown in Table 5.

6 Simulation and results

To evaluate the effectiveness of the developed fault-tolerant power management algorithm, we cause, on purpose, two temporary faults, F1 and F2, and one permanent fault, F3, as listed below:

F1: Temporary fault occurs in FC at 84s and lasts 5s.
F2: Temporary fault occurs in SC at 300s and lasts 5s.
F3: Permanent fault occurs in FC and persists till the end of the ride.

Figure 11 shows the HEV speed along with the reference speed applied for the HEV during the 660s. It is clear that the HEV speed tracks well its reference. Figure 12 shows the HEV torque response. The vehicle torque matches its reference, and the torque ripples are minimized in a narrow hysteresis band.

Initial control signals, final control signals, and fault signals generated are shown in Figure 13. One can notice that during normal operation, the final control signals A and B are the initial control signals image of N_{SC} and $N_{FC,}$ respectively,

generated by the power management algorithm. When a failure occurs in either SC or FC, the fault detection bloc detects the fault, and the isolation bloc uses the truth table in Table 5 to determine whether to isolate the faulty source and to keep the DC bus voltage at its reference.

- At F1: "C^F_{SC}" stays at 1 to let the SC fix the DC bus voltage, and "C^F_{FC}" toggles from 4 to 3 to disconnect the faulty FC. At the end of the temporary fault, the signal C^F_{SC} returns to its previous state, which is 4.
- At F2: "C^F_{SC}" goes from 1 to 3 to disconnect the SC, and "C^F_{FC}" toggles from 4 to 1 to enable the FC to fix the DC bus

TABLE 4 Different driving rules.

Mode	Power	SOCsc	Active sources	N_{FC}	N_{SC}	Mode
$p > 0$	P_L	SOC_H	SC only	3	1	1
		SOC_A	FC only	1	3	2
		SOC_C	FC + slow SC charge	1	2	3
		SOC_L	FC + fast SC charge	1	2	4
	P_A	SOC_H	SC only	3	1	5
		SOC_A	FC 50%, SC 50%	4	1	6
		SOC_C	FC 70%, SC 30%	2	1	7
		SOC_L	FC + fast SC charge	1	2	8
	P_H	SOC_H	FC 50%, SC 50%	4	1	9
		SOC_A	FC 50%, SC 50%	4	1	10
		SOC_C	FC 70%, SC 30%	2	1	11
		SOC_L	FC + fast SC charge	1	2	12
$p < 0$	P_N	—	SC charge	3	1	13

TABLE 5 Fault correction truth table.

F_{SC}	F_{SC}	C^F_{FC}	C^F_{SC}	SW1	SW2
0	0	C_{FC}	C_{SC}	Closed	Closed
0	1	1	3	Closed	Open
1	0	3	1	Open	Closed

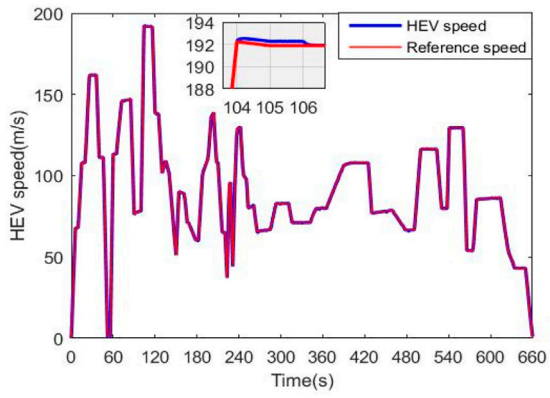

FIGURE 11
HEV speed response.

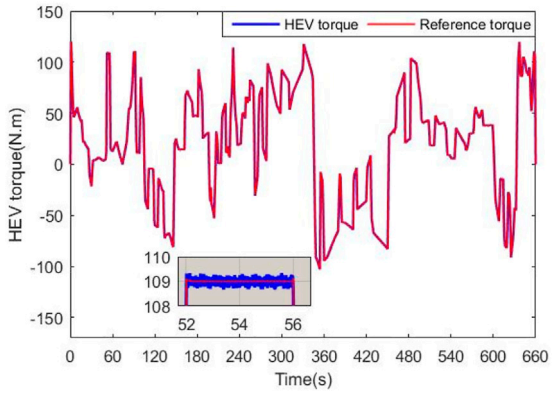

FIGURE 12
HEV torque response.

voltage. After the end of fault at 305s, C^F_{FC} and C^F_{SC} recover their previous values, 4 and 1, respectively.

- At F3: "C^F_{SC}" goes from 3 to 1 to enable the SC to regulate the DC bus voltage because the FC is in a failure state. The correction bloc also toggles "C^F_{FC}" from 1 to 3 to disconnect the faulty FC. In this case, the control signals are kept in this position till the end of the ride since the fault is assumed to be permanent.

One can also remark on the effectiveness of the fault detection bloc, which did not emit any false threshold signal and responded immediately to the different faults.

Figure 14 shows the HEV, SC power, and FC power. It can be seen that the HEV power, at each instant, is obtained as the sum of SC and FC powers. It can be seen that during fault situations (F1, F2, and F3), the non-faulty source ensures HEV traction and the faulty source is isolated.

To provide a closer look at the behavior of power sources during vehicle ride, Figure 15 shows the SC and FC power along with the driving mode number during the period [75.5s and 92.5s].

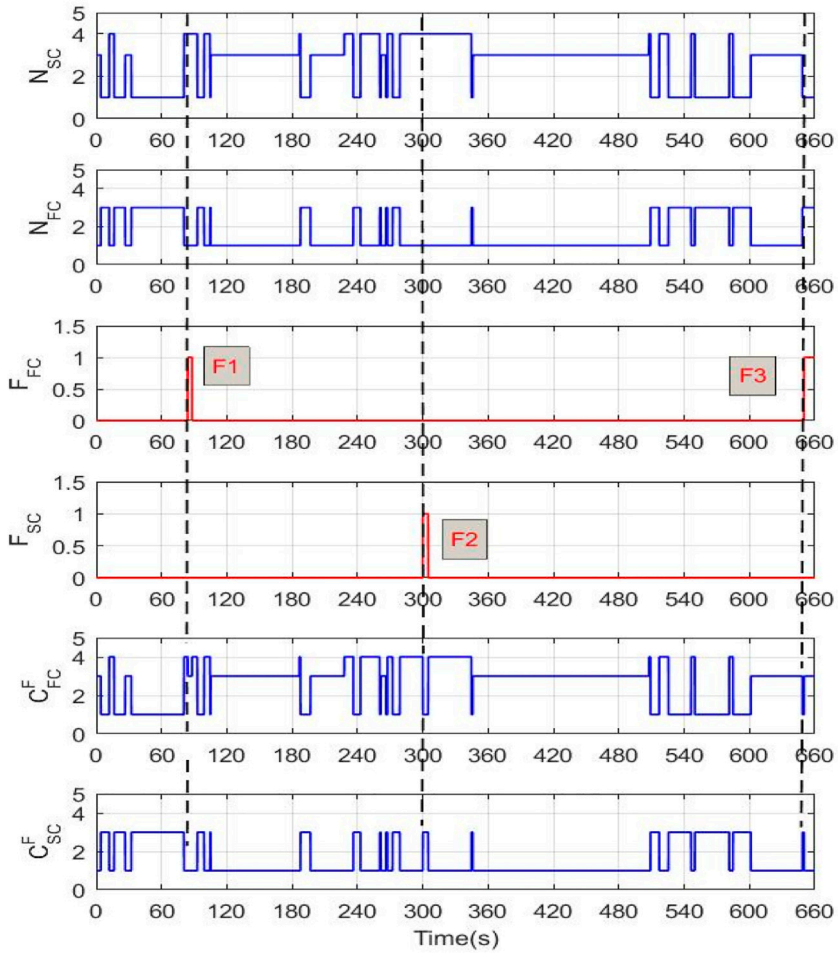

FIGURE 13
Fault and control signals during HEV ride.

- During [75.5, t_1]: During this time period, $SOC_{SC} = SOC_N$ and HEV power demand is low. Following Table 4, FC will ensure HEV traction while fixing DC bus voltage ($C^F_{FC} = 1$), and the SC will be turned OFF ($C^F_{SC} = 3$).
- During [t_1, t_2]: In this time interval, HEV power demand is average, and SOC_{SC} belongs to SOC_N. In this case, both FC and SC will provide 50% of the total power required for traction, as shown in Figure 15, where both sources deliver half of the load power applied on the HEV
- During [t_2, t_3] U [t_4, t_5]: During this time period, HEV power demand is high, and the SC state of charge belongs to SOC_N. Hence, FC and SC deliver 50% of the required traction power for traction, as highlighted in Figure 15, where both sources deliver 4 kW.
- During [t_3, t_4]: In this time interval, a fault occurs at the FC level, while HEV power demand is high and SOC_{SC} belongs to SOC_N. The fault detection and correction block, shown in Figure 8, overwrite the decision of the power management algorithm to ensure continuous HEV operation and DC bus regulation. This is achieved through the reconfiguration of the SC control scheme to position 1 ($C^F_{SC} = 1$) and the FC control loop to position 3 ($C^F_{FC} = 1$).

Figure 16 shows the SC SOC. It dropped from 82 to 70% during [210s, 350s], which corresponds to an average- and high-power demand. During the regenerative braking period [350,450], SOC_{SC} increased from 70 to 86%. Globally, the SOC_{SC} stayed within safe limits during the ride.

Figure 17 highlights the inverter DC bus voltage. One can notice that it follows its reference set to 560 V. The presence of some voltage ripples due to connection and disconnection of power sources can be remarked. These ripples are within an allowed band of 10 V. The zooms in Figure 17 present the voltage fluctuations during the occurrence of faults. These fluctuations are always within safe limits.

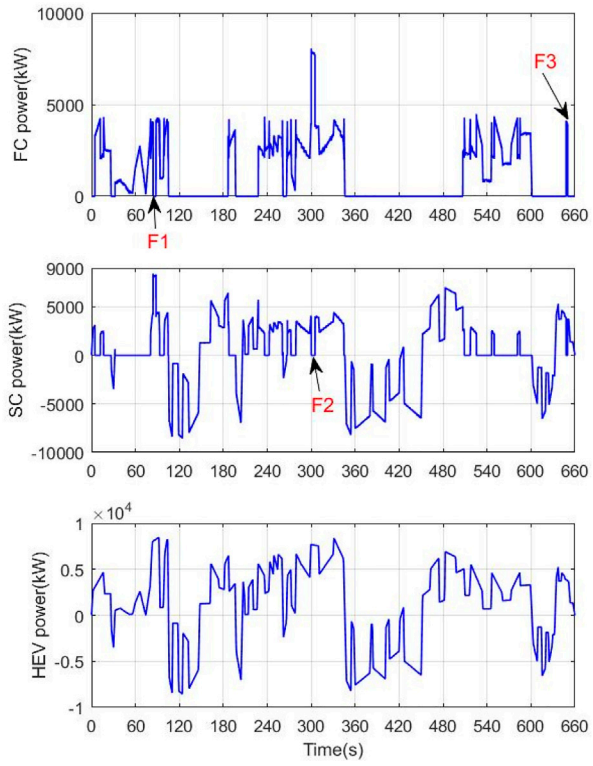

FIGURE 14
SC, FC, and HEV powers.

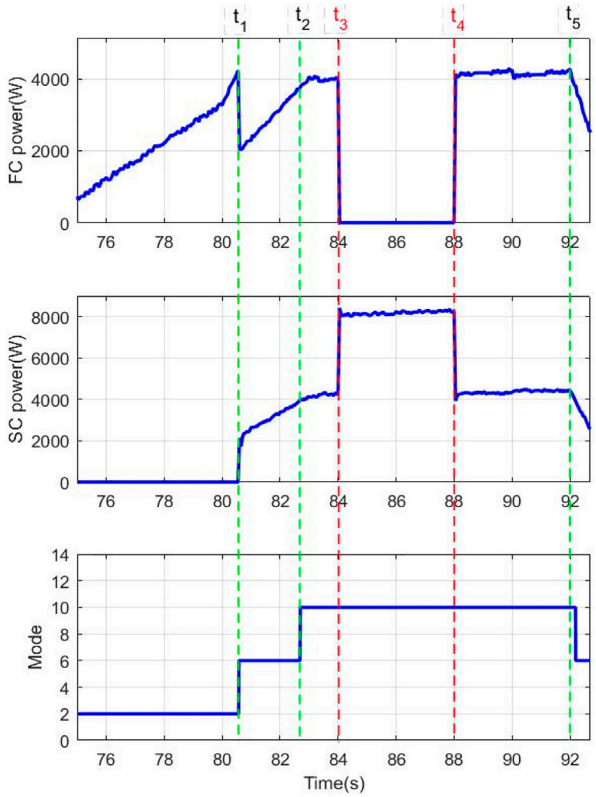

FIGURE 15
SC, FC, and HEV powers.

The minimum cost after each iteration is shown at 18. It can be seen that cost decreases over iterations, which means that the solutions produced after each generation are better than the previous ones in term of torque and speed ripple minimization. Starting from 30, the cost value is constant, which means that the PSO algorithm converges to an optimum solution.

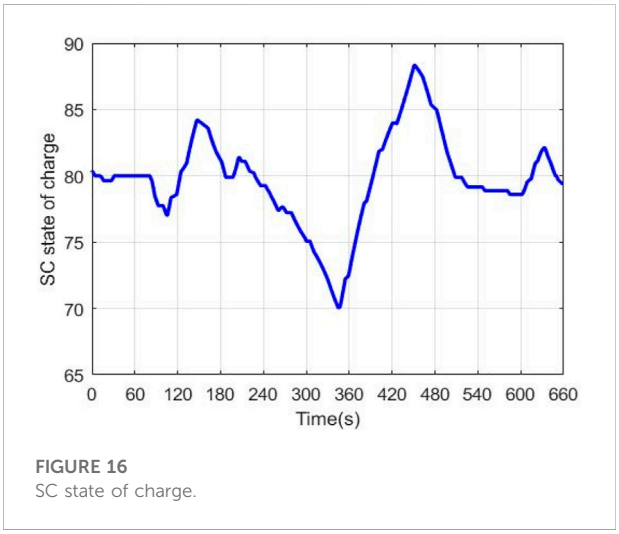

FIGURE 16
SC state of charge.

7 Real-time validation

The effectiveness of the proposed energy management strategy is assessed by implementing it in real-time using the OPAL-RT LAB simulator. Figure 18 describes in detail how the HEV model is adapted for simulation on the aforementioned simulation platform. The first step toward RT simulation is model separation. It should be divided into computation and console blocks, which are highlighted with blue and dark dashed lines, respectively, in Figure 18. The console block contains user interface blocks such as scopes, displays, manual switches, and constants. It is worth noticing that the console block runs asynchronously only on the host PC from the computation subsystems. The computational subsystem contains all the computational elements of the model, mathematical operations, I/O blocks, signal generators, and physical models. Data between the computation subsystem and console are

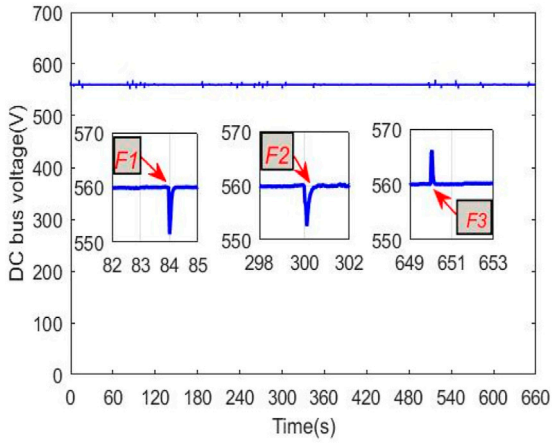

FIGURE 17
DC bus voltage.

exchanged asynchronously through the TCP/IP link, but data exchange between two computation subsystems, namely, master (SM) and slave (SS), is performed synchronously through shared memory. Data from the RT simulator are displayed on the digital oscilloscope using Bayonet Neill–Concelman connector (BNC) to BNC cable.

After building and loading the HEV program to the OP 57000 simulator, constant power of 5 kW is applied as a load power to the vehicle. This requested power will be ensured by FC and SC following the proposed energy management strategy. Figure 19 shows the obtained results using the RT LAB simulator, where fuel cell and supercapacitor powers are highlighted with magenta and blue colors, respectively. The aforementioned figure confirms the facts stated in section 5 where it has been said that the fuel cell can be operated safely at different predefined operating points. In zone 1 (Z1), the supercapacitor delivers all the necessary power for traction while the fuel cell is turned off by setting its control loop to position 3, as shown in Figure 9. In zone 2 (Z2), FC and SC control loops were set to positions 4 and 1, respectively. This last-mentioned control loop configuration has made both FC and SC deliver 50% of the required power for traction. It is worth noticing that SC in Z2 delivers 50% of the required power for traction while ensuring DC bus regulation. At Z3, a temporary fault took place at the FC level. As soon as the fault occurs at the fuel cell level, as pointed out with white dashed lines, the fault detection and correction block, already shown in

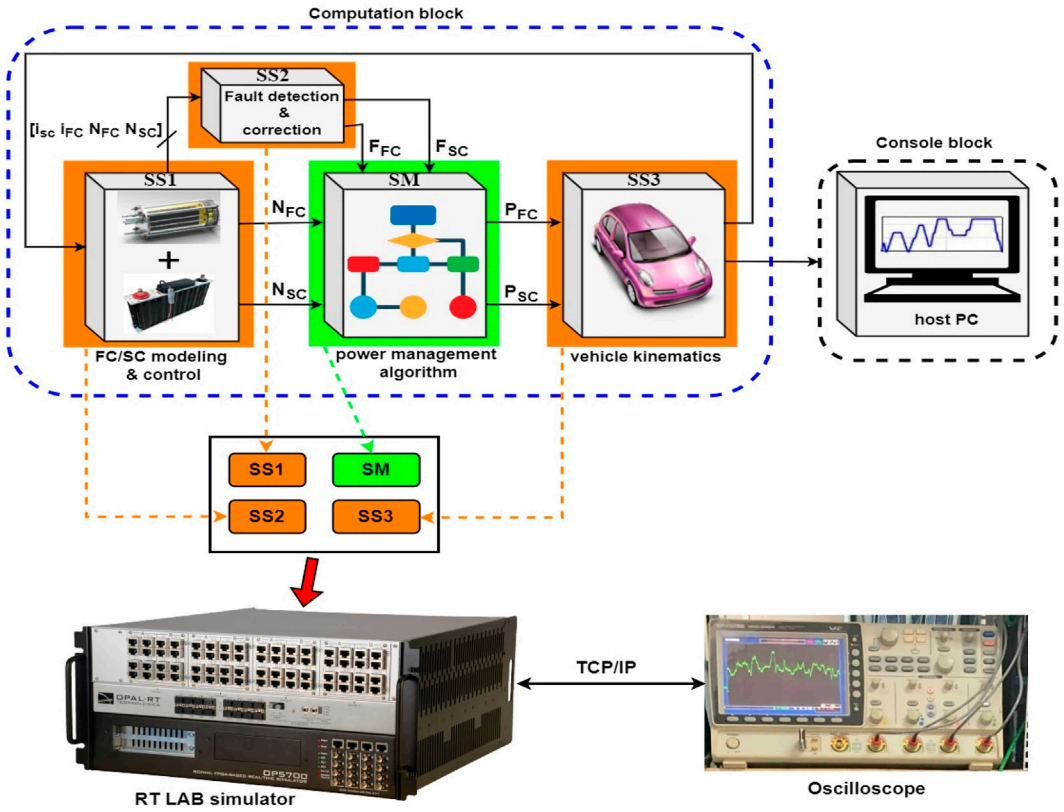

FIGURE 18
Real-time simulation using RT LAB.

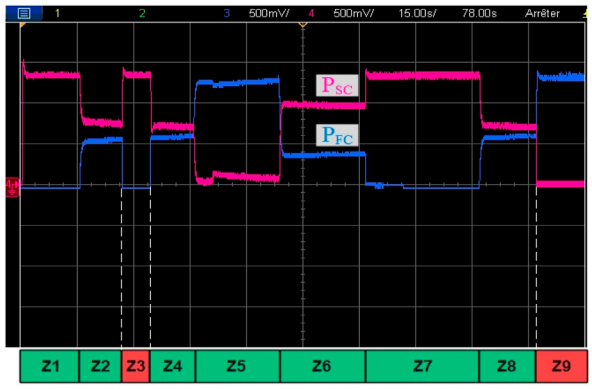

FIGURE 19
Real-time simulation using RT LAB.

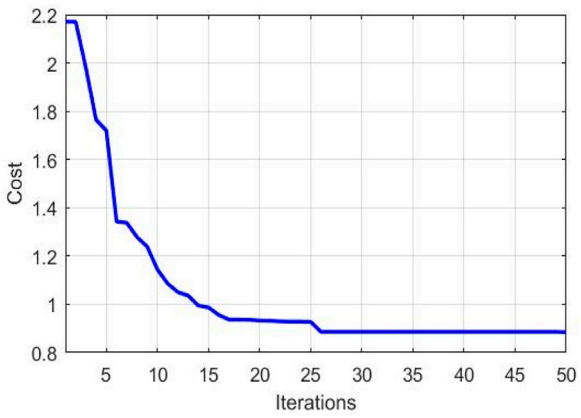

FIGURE 20
Evolution of cost over iterations.

Figure 20, will intervene to isolate the FC and overwrite the power management algorithm by forcing FC power to zero. This is performed by the reconfiguration of the FC control loop from position 4 to position 3, as shown in Figure 9. This will make the supercapacitor deliver, alone, all the power required for traction while ensuring DC bus regulation. From zone 4 to 8, one can see that the fuel cell delivers a percentage of total power that is equal to the power contribution factor C_{FC}. For example, in zones 4, 5, and 6, the fuel cell delivers respectively 50, 100, and 30% of the required power for traction. One of the advantages of such a power management technique is the precise control of power flow in power sources. In addition to that, this power management strategy reduces the stress applied on power sources by preventing their operation above their maximum power. In zone 9, a fault occurred at the SC level, which is responsible for DC bus regulation. The fault detection and correction block shown in Figure 20 has isolated SC by reconfiguring its control loop shown in Figure 9 from position 1 to position 3. Furthermore, the FC control loop was set to position 1 to ensure DC bus regulation and deliver all the necessary power for traction.

8 Conclusion

The developed power management strategy has improved HEV security since failures in vehicle power sources are detected and isolated. HEV reliability and comfort are also enhanced because both SC and FC are able to regulate the DC bus voltage, power the HEV alone, and operate at different power levels. The offline use of PSO in the design of HEV controllers has made the controller design task easy and automatic *via* the use of a proposed cost function that trades between design variables to be minimized.

Data availability statement

The original contributions presented in the study are included in the article/Supplementary Material; further inquiries can be directed to the corresponding author.

Author contributions

All authors listed have made a substantial, direct, and intellectual contribution to the work and approved it for publication.

Conflict of interest

The authors declare that the research was conducted in the absence of any commercial or financial relationships that could be construed as a potential conflict of interest.

Publisher's note

References

He, H., Quan, S., Sun, F., and Wang, Y. X. (2020). Model predictive control with lifetime constraints based energy management strategy for proton exchange membrane fuel cell hybrid power systems. *IEEE Trans. Ind. Electron.* 67 (10), 9012–9023. doi:10.1109/TIE.2020.2977574

Hwang, J. J., Chen, Y. J., and Kuo, J. K. (2012). The study on the power management system in a fuel cell hybrid vehicle. *Int. J. hydrogen energy* 37 (5), 4476–4489. doi:10.1016/j.ijhydene.2011.11.127

Jnayah, S., and Khedher, A. (2019). "DTC of induction motor drives fed by two and three-level inverter: Modeling and simulation," in *2019 19th international conference on sciences and techniques of automatic control and computer engineering (STA)* (IEEE). doi:10.1109/STA.2019.8717227

Kakouche, K., Rekioua, T., Mezani, S., Oubelaid, A., Rekioua, D., Blazek, V., et al. (2022). Model predictive direct torque control and fuzzy logic energy management for multi power source electric vehicles. *Sensors* 22, 5669. doi:10.3390/s22155669

Kaplan, H., Tehrani, K., and Jamshidi, M. (2021). A fault diagnosis design based on deep learning approach for electric vehicle applications. *Energies* 14 (20), 6599. doi:10.3390/en14206599

Kersten, A., Oberdieck, K., Bubert, A., Neubert, M., Grunditz, E. A., Thiringer, T., et al. (2019). Fault detection and localization for limp home functionality of three-level NPC inverters with connected neutral point for electric vehicles. *IEEE Trans. Transp. Electrific.* 5 (2), 416–432. doi:10.1109/tte.2019.2899722

Kommuri, S. K., Defoort, M., Karimi, H. R., and Veluvolu, K. C. (2016). A robust observer-based sensor fault-tolerant control for PMSM in electric vehicles. *IEEE Trans. Ind. Electron.* 63 (12), 7671–7681. doi:10.1109/tie.2016.2590993

Koprivsek, M. (2018). "Advanced solutions in over-current protection of hvdc circuit of battery-powered electric vehicle," in *PCIM europe 2018; international exhibition and conference for power electronics, intelligent motion* (Nuremberg, Germany: Renewable Energy and Energy ManagementVDE), 1–4.

Liu, J., Li, H., and Deng, Y. (2017). Torque ripple minimization of PMSM based on robust ILC via adaptive sliding mode control. *IEEE Trans. Power Electron.* 33 (4), 3655–3671. doi:10.1109/TPEL.2017.2711098

Liu, X., Yu, F., Mao, J., and Yang, H. (2021). Pre-and post-fault operations of six-phase electric-drive-reconstructed onboard charger for electric vehicles. *IEEE Trans. Transp. Electrific.* 8 (2), 1981–1993. doi:10.1109/tte.2021.3113316

Max, G., and Lantos, B. (2014). Time optimal control of four-in-wheel-motors driven electric cars. *Period. Polytech. elec. Eng. Comp. Sci.* 58 (4), 149–159. doi:10.3311/PPee.7806

Mellor, P. H., Allen, T. J., Ong, R., and Rahma, Z. (2003). Faulted behaviour of permanent magnet electric vehicle traction drives. *IEEE Int. Electr. Mach. Drives Conf.* 1, 554–558.

Meyer, R. T., Johnson, S. C., DeCarlo, R. A., Pekarek, S., and Sudhoff, S. D. (2018). Hybrid electric vehicle fault tolerant control. *J. Dyn. Syst. Meas. Control* 140 (2). doi:10.1115/1.4037270

Moosavi, S. S., Kazemi, A., and Akbari, H. (2019). A comparison of various open-circuit fault detection methods in the IGBT-based DC/AC inverter used in electric vehicle. *Eng. Fail. Anal.* 96, 223–235. doi:10.1016/j.engfailanal.2018.09.020

Ou, K., Wang, Y. X., and Kim, Y. B., (2017). Performance optimization for open-cathode fuel cell systems with overheating protection and air starvation prevention. *Fuel Cells* 17, 299. doi:10.1002/fuce.201600181

Ou, K., Yuan, W. W., Choi, M., Kim, J., and Kim, Y. B. (2019). Development of new energy management strategy for a household fuel cell/battery hybrid system. *Int. J. Energy Res.* 43 (9), 4686–4700. doi:10.1002/er.4606

Oubelaid, A., Albalawi, F., Rekioua, T., Ghoneim, S. S., Taib, N., and Abdelwahab, S. A. M. (2022). Intelligent torque allocation based coordinated switching strategy for comfort enhancement of hybrid electric vehicles. *IEEE Access* 10, 58097–58115. doi:10.1109/ACCESS.2022.3178956

Oubelaid, A., Alharbi, H., B Humayd, A. S., Taib, N., Rekioua, T., and Ghoneim, S. S. M. (2022). Fuzzy-energy-management-based intelligent direct torque control for a battery—supercapacitor electric vehicle. *Sustainability* 14, 8407. doi:10.3390/su14148407

Oubelaid, A., Taib, N., Nikolovski, S., Alharbi, T. E. A., Rekioua, T., Flah, A., et al. (2022). Intelligent speed control and performance investigation of a vector controlled electric vehicle considering driving cycles. *Electronics* 11 (13), 1925. doi:10.3390/electronics11131925

Oubelaid, A., Taib, N., and Rekioua, T. (2022). "Novel coordinated power sources switching strategy for transient performance enhancement of hybrid electric vehicles," in *COMPEL-The international journal for computation and mathematics in electrical and electronic engineering*. doi:10.1108/COMPEL-10-2021-0399

Peñate, S. G., Estrada, F. R. L., Palomo, G. V., Ríos, R. O., Hernández, J. A. Z., Rojas, C. R., et al. (2018). Sensor fault diagnosis observer for an electric vehicle modeled as a Takagi-Sugeno system. *J. Sensors*, 1–9. doi:10.1155/2018/3291639

Raghavaiah, K., and Srinivasarao, G., (2019), Design and simulation of a controller for a hybrid energy storage system based electric vehicle, *Math. Model. Eng. Problems*, 6 (2), 203–216. doi:10.18280/mmep.060208

Sabaliauskaite, G., Liew, L. S., and Zhou, F. (2019). "AVES–Automated vehicle safety and security analysis framework," in *ACM computer science in cars symposium*, 1–8. doi:10.1145/3359999.3360494

Shchurov, N. I., Dedov, S. I., Malozyomov, B. V., Shtang, A. A., Martyushev, N. V., Klyuev, R. V., et al. (2021). Degradation of lithium-ion batteries in an electric transport complex. *Energies* 14 (23), 8072. doi:10.3390/en14238072

Song, K., Ding, Y., Hu, X., Xu, H., Wang, Y., and Cao, J. (2021). Degradation adaptive energy management strategy using fuel cell state-of-health for fuel economy improvement of hybrid electric vehicle. *Appl. Energy* 285, 116413. doi:10.1016/j.apenergy.2020.116413

Tao, F., Zhu, L., Fu, Z., Si, P., and Sun, L. (2020). Frequency decoupling-based energy management strategy for fuel cell/battery/ultracapacitor hybrid vehicle using fuzzy control method. *IEEE Access* 8, 166491–166502. doi:10.1109/ACCESS.2020.3023470

Tashakori, A., and Ektesabi, M. (2013). Fault diagnosis of in-wheel BLDC motor drive for electric vehicle application. *2013 IEEE Intell. Veh. Symp.* IV, 925–930.

Thounthong, P., Rael, S., and Davat, B. (2009). Analysis of supercapacitor as second source based on fuel cell power generation. *IEEE Trans. Energy Convers.* 24 (1), 247–255. doi:10.1109/TEC.2008.2003216

Trinh, H. A., and Ahn, K. K. (2021). "Energy management strategy for fuel cell hybrid power system using fuzzy logic and frequency decoupling methods," in *2021 24th international conference on mechatronics technology* (Singapore: ICMT), 1–6. IEEE. doi:10.1109/ICMT53429.2021.9687291

Vajsz, T., Számel, L., and Rácz, G. (2017). A novel modified DTC-SVM method with better overload-capability for permanent magnet synchronous motor servo drives. *Period. Polytech. elec. Eng. Comp. Sci.* 61 (3), 253–263. doi:10.3311/PPee.10428

Wieczorek, M., and Lewandowski, M. (2017). A mathematical representation of an energy management strategy for hybrid energy storage system in electric vehicle and real time optimization using a genetic algorithm. *Appl. energy* 192, 222–233. doi:10.1016/j.apenergy.2017.02.022

Wu, C., Sehab, R., Akrad, A., and Morel, C. (2022). Fault diagnosis methods and Fault tolerant control strategies for the electric vehicle powertrains. *Energies* 15 (13), 4840. doi:10.3390/en15134840

Wu, G., Zhang, X., and Dong, Z. (2015). Powertrain architectures of electrified vehicles: Review, classification and comparison. *J. Frankl. Inst.* 352 (2), 425–448. doi:10.1016/j.jfranklin.2014.04.018

Xie, S., Hu, X., Qi, S., and Lang, K. (2018). An artificial neural network-enhanced energy management strategy for plug-in hybrid electric vehicles. *Energy* 163, 837–848. doi:10.1016/j.energy.2018.08.139

Yadav, K., and Maurya, S. (2022). "A comparative study on the performance of energy storage systems for hybrid electric vehicles," in *Advances in energy technology* (Singapore: Springer), 795–803.

Yadav, K., and Maurya, S. (2021). "Fuzzy control implementation for energy management in hybrid electric vehicle," in *2021 international conference on computer communication and informatics (ICCCI)* (IEEE), 1–5.

Yadav, K., and Maurya, S. K. (2021). "Modelling and control of power flow from auxiliary source in hybrid electric vehicle," in *Recent advances in power electronics and drives* (Singapore: Springer), 217–227.

Yi, F., Lu, D., Wang, X., Pan, C., Tao, Y., Zhou, J., et al. (2022). Energy management strategy for hybrid energy storage electric vehicles based on pontryagin's minimum principle considering battery degradation. *Sustainability* 14 (3), 1214. doi:10.3390/su14031214

Yu, L., Zhang, Y., Huang, W., and Teffah, K. (2017). A fast-acting diagnostic algorithm of insulated gate bipolar transistor open circuit faults for power inverters in electric vehicles. *Energies* 10 (4), 552. doi:10.3390/en10040552

Yu, Q., Wan, C., Li, J., Xiong, R., and Chen, Z. (2021). A model-based sensor fault diagnosis scheme for batteries in electric vehicles. *Energies* 14 (4), 829. doi:10.3390/en14040829

Zhang, D., Liu, G., Zhou, H., and Zhao, W. (2018). Adaptive sliding mode fault-tolerant coordination control for four-wheel independently driven electric vehicles. *IEEE Trans. Ind. Electron.* 65 (11), 9090–9100. doi:10.1109/TIE.2018.2798571

Zhang, L., Fan, Y., Cui, R., Lorenz, R. D., and Cheng, M. (2017). Fault-tolerant direct torque control of five-phase FTFSCW-IPM motor based on analogous three-phase SVPWM for electric vehicle applications. *IEEE Trans. Veh. Technol.* 67 (2), 910–919. doi:10.1109/TVT.2017.2760980

Zhang, L., Wang, Z., Ding, X., Li, S., and Wang, Z. (2021). Fault-tolerant control for intelligent electrified vehicles against front wheel steering angle sensor faults during trajectory tracking. *IEEE Access* 9, 65174–65186. doi:10.1109/access.2021.3075325

Zhang, S., Xiong, R., and Sun, F. (2017). Model predictive control for power management in a plug-in hybrid electric vehicle with a hybrid energy storage system. *Appl. Energy* 185, 1654–1662. doi:10.1016/j.apenergy.2015.12.035

Zhang, Z., Guan, C., and Liu, Z. (2020). Real-time optimization energy management strategy for fuel cell hybrid ships considering power sources degradation. *IEEE Access* 8, 87046–87059. doi:10.1109/ACCESS.2020.2991519

Nomenclature

Abbreviations

AASE Average absolute speed error

AATE Average absolute torque error

Ang Angle

DC Direct current

D Decision signal

DTC Direct torque control

FC Fuel cell

HEV Hybrid electric vehicle

PMSM Permanent magnet synchronous machine

PSO Particle swarm optimization

RT Real-time

SC Supercapacitor

SVM Space vector modulation

$\mathbf{S_{ABC}}$ Inverter gate signals

Symbols

$\boldsymbol{a}$ Vehicle acceleration [m/s^2]

$\mathbf{E_{nernst}}$ Nernst voltage [V]

$\mathbf{F_{traction}}$ External force [N]

$\mathbf{F_r}$ Resistive force [N]

$\mathbf{F_{aero}}$ Aerodynamic force [N]

$\mathbf{F_g}$ Gravitational force [N]

$\mathbf{F_{tire}}$ Tire force [N]

$\mathbf{F_{acc}}$ Acceleration force [N]

$\mathbf{i_{SC}}$ Supercapacitor current [A]

$\boldsymbol{m}$ Vehicle mass [kg]

$\mathbf{i_d}$ Direct axis current [A]

$\mathbf{i_q}$ Quadratic axis current [A]

i_α Alpha axis current [A]

i_β Beta axis current [A]

L Stator inductance [H]

$\mathbf{N_s}$ Number of series fuel cells

$\mathbf{N_{sc}}$ Number of series supercapacitors

$\mathbf{P_{FC}}$ Fuel cell power [kW]

$\boldsymbol{Q_{init}}$ Initial supercapacitor charge [C]

$\boldsymbol{Q_T}$ Total supercapacitor charge [C]

$\mathbf{P_{SC}}$ Supercapacitor power [kW]

$\mathbf{r_{sc}}$ Supercapacitor series resistance [Ω]

$\mathbf{SOC_{SC}}$ Supercapacitor state of charge

$\mathbf{V_{FC,\ cell}}$ Fuel cell voltage [V]

$\mathbf{V_{FC}}$ Fuel cell stack voltage [V]

$\mathbf{V_{act}}$ Activation voltage drop [V]

$\mathbf{V_{ohm}}$ Ohmic voltage drop [V]

$\mathbf{V_{cond}}$ Conduction voltage drop [V]

$\mathbf{V_{SC}}$ Supercapacitor voltage [V]

$\mathbf{V_{SC,tot}}$ Supercapacitor total voltage [V]

$\mathbf{V_T}$ Terminal voltage [V]

ϕ Permanent magnet flux [Wb]

λ_d Direct axis flux linkage [V]

λ_q Quadratic axis flux linkage [V]

$\mathbf{V_d}$ Direct axis voltage [V]

$\mathbf{V_q}$ Quadratic axis voltage [V]

p Number of poles

w_r Motor angular frequency [rad/s]

P Motor power [kW]

$\mathbf{T_n}$ Motor nominal torque [N]

$\mathbf{r_s}$ Motor stator resistance [Ω]

J Rotor inertia [kg.m^2]

B Rotor viscous friction [N.m.s]

ϕ_α Alpha axis flux [Wb]

ϕ_β Beta axis flux [Wb]

$\mathbf{T_S}$ Sampling time [s]

V_α Alpha axis voltage [V]

V_β Beta axis voltage [V]

ϕ_{es} Estimated flux [Wb]

T_{es} Estimated torque [N.m]

θ_s Estimated flux angle [°]

$\mathbf{V_{DC}}$ DC bus voltage [V]

$\mathbf{C_{bus}}$ Bus capacitor [F]

$\mathbf{\Omega_i}$ Reference speed at ith iteration [rad/s]

$\mathbf{T_i}$ Reference torque at ith iteration [N.m]

N Torque and speed vectors length

T_d Speed profile duration [s]

e_T Torque error [N.m]

e_s Speed error [rad/s]

v_i^t Particle's velocity

w_t Inertia factor

c_1,c_2 Cognitive and swarm influence

r_1,r_2 Random numbers

P_{best}^t Personal best

G^t_{best} Global best

x^t_i Particle's position in the swarm

C_{FC} Initial fuel cell control signal

C_{SC} Initial supercapacitor control signal

C^F_{FC} Final fuel cell control signal

C^F_{SC} Final supercapacitor control signal